Published on 24 August 2016. Downloaded by National Institutes of Standards & Technology on 22/05/2017 20:20:39.

Soft Matter

PAPER

View Article Online
View Journal | View Issue

Cite this: *Soft Matter*, 2016, 12, 7863

Tuning the bridging attraction between large hard particles by the softness of small microgels†

Junhua Luo,[ab] Guangcui Yuan*[acd] and Charles C. Han*[ae]

Received 3rd July 2016,
Accepted 23rd August 2016

DOI: 10.1039/c6sm01519k

www.rsc.org/softmatter

In this study, the attraction between large hard polystyrene (PS) spheres is studied by using three types of small microgels as bridging agents. One is a purely soft poly(*N*-isopropylacrylamide) (PNIPAM) microgel, the other two have a non-deformable PS hard core surrounded by a soft PNIPAM shell but are different in the core–shell ratio. The affinity for bridging the large PS spheres is provided and thus affected by the PNIPAM constituent in the microgels. The bridging effects caused by the microgels can be indirectly incorporated into their influence on the effective attraction interaction between the large hard spheres, since the size of the microgels is very small in comparison to the size of the PS hard spheres. At a given volume fraction of large PS spheres, they behave essentially as hard spheres in the absence of small microgels. By gradually adding the microgels, the large spheres are connected to each other through the bridging of small particles until the attraction strength reaches a maximum value, after which adding more small particles slowly decreases the effective attraction strength and eventually the large particles disperse individually when saturated adsorption is achieved. The aggregation and gelation behaviors triggered by these three types of small microgels are compared and discussed. A way to tune the strength and range of the short-range attractive potential *via* changing the softness of bridging microgels (which can be achieved either by using core–shell microgels or by changing the temperature) is proposed.

Introduction

Colloidal particles with short-range attraction (the range of the attractive interparticle interaction is a few percent of the particle diameter) can form disordered solids in various ways depending on the effective interaction potential (U) and the volume fraction of particles (Φ).[1,2] Two extreme cases are hard sphere colloidal glasses at high Φ and low U, and strongly attractive colloidal gels at low Φ and high U. Theoretically, there are different models to incorporate the short-range attraction, such as the hard-core attractive Yukawa interaction[3–6] that represents the screened electric potential, the Asakura–Oosawa potential[7,8] that takes into account the effect of depletion forces in colloid–polymer mixtures, the Lennard-Jones potential[9,10] used in the description of protein–protein interactions, Baxter's sticky hard-sphere model[11–13] that assumes an infinitely deep attraction at close contact, and the square-well potentials[14] which account for excluded volume effects associated with the hard-core diameter (σ) plus an attractive layer of width (Δ) and strength (ε). It is generally assumed that the detailed shapes of the short-range attractive potentials are rather unimportant in determining the global features of the phase diagram. Therefore, Noro and Frenkel[15] suggested to use a reduced second virial coefficient (B_2^*) as a convenient parameter to quantify the effective interaction of any arbitrary attractive potential. The effective interaction of an arbitrary attractive potential can be equal to the equivalent square-well fluid that yields the same B_2^* at the same reduced temperature $T^* = k_BT/\varepsilon$. In this way, one can estimate the relative location of the thermodynamics liquid–solid transition curves by the knowledge of B_2^*. The scaling of structural and dynamical properties with the range of interaction has been a research focus in the field of colloid physics.[5,6,10,15–18] Computer simulations studying the isodiffusivity indicated that gelation at a volume fraction less than the critical concentration, which is around 0.266 for a sticky hard sphere system,[13] should be driven by the frustrated gas–liquid separation.[18]

Experimentally, there are different colloidal systems available for studying the effects of short-range attraction on the

[a] *Beijing National Laboratory for Molecular Sciences, Institute of Chemistry, Chinese Academy of Sciences, Beijing 100190, China. E-mail: c.c.han@iccas.ac.cn; Tel: +86-10-82618089*
[b] *University of Chinese Academy of Sciences, Beijing 100049, China*
[c] *Center for Neutron Research, National Institute of Standards and Technology, Gaithersburg, Maryland 20899, USA. E-mail: guangcui.yuan@nist.gov; Tel: +1 (301)-975-5098*
[d] *Department of Polymer Engineering, The University of Akron, Akron, Ohio 44325, USA*
[e] *Institute for Advanced Study, Shenzhen University, Shenzhen 518060, China*

† Electronic supplementary information (ESI) available. See DOI: 10.1039/c6sm01519k

Published on 24 August 2016. Downloaded by National Institutes of Standards & Technology on 22/05/2017 20:20:39.

dynamical arrested behaviors (gelation and glass transition). Accordingly, there are various ways to tune the attractive interaction between the colloidal particles. One example is charge stabilized colloidal particles (such as polystyrene latex[19]) with an added electrolyte. The attraction originates from the London–van der Waals dispersion forces when the stabilizing electrostatic repulsive forces from the surface charges are screened by the addition of an electrolyte. Another type of system consists of colloidal particles with a grafted thermal (or solvent-quality) sensitive surface layer. The collapse[20,21] or solidification transition[22] of the brush under different environments leads to a variable short-range attraction between the particles. Protein suspensions are also used as model systems exhibiting short-range attractions, because the phase behavior can be tuned either by addition of salts (which may modify the pH) or by temperature variation.[23,24] The most widely used model systems are mixed suspensions of colloids and non-adsorbing polymers, in which the entropy-driven depletion effect will produce an effective attraction potential between large particles. A notable example is sterically stabilized poly(methyl methacrylate) particles suspended in organic media with polystyrene as a depleting agent.[25] The range and depth of depletion potential can be adjusted by the size ratio and free volume concentration of the non-adsorbing polymer, respectively.[7,25] Experiments on this depletion attraction system demonstrated that gelation transitions at volume fractions up to about 0.16 indeed follow the gas–liquid phase transition line,[26] as predicted by computer simulation.[18] This conclusion has been widely considered a general theory for gelation transitions of spherical colloidal systems with different origins of short-ranged attraction.[24,26]

If no dynamical ingredients (such as bond lifetime) are taken into account, a thermodynamics generalization is feasible.[27] However, the kinetic effects on gelation transitions of real experimental systems cannot be ignored, although they are hard to quantify. People need to be prudent when generalizing the physical picture of the gelation transitions obtained from systems with different origins of effective attraction between colloidal particles. Let us consider two extreme cases with short-range attraction: the depletion attraction driven system and the bridging attraction driven system. We assume that the radius of gyration of an added polymer (or particle) is much smaller than the colloidal size. Then, the depletion attraction driven system and bridging attraction driven system will share some similarities in that they are both binary systems with a large asymmetric size ratio between two types of particles. The only difference between these two systems is the interaction between the small particles and large particles. There is no attraction between the small particles and large particles in the depletion system, while the attraction between the small particles and large particles in the bridging system is very strong. In the depletion attraction system, as mentioned above,[26] the gelation transition is generally believed to be related with only thermodynamic equilibrium gas–liquid separation (frustrated spinodal separation), not a purely kinetic phenomenon. However, in the bridging attraction system, as we have recently demonstrated,[28] the gelation transition at the intermediate range volume fraction is a more kinetic driven effect (follows more closely the percolation line), even though at a small volume fraction (less than 10%), gelation seems to follow the gas–liquid transition line.[29] This striking contrast between depletion and bridging systems indicates that the attraction force between the added small particles and the colloidal particles (or maybe the details of attractive potentials) play much bigger roles than people previously assumed. By changing the attraction strength between the added small particles and the colloidal particles, it might be possible that in some cases, both the kinetic effect and the frustrated liquid–gas separation may play equally important roles at different stages of the gelation transition.

There are many binary colloidal systems in which the attraction strengths between the small particles and the large particles fall right in between the two above-mentioned extreme cases. Therefore, it is interesting to tune the attractive interaction between the small particles and large particles, and then to investigate its effect on the gelation behaviours. However, this is very challenging and has not been widely studied. Dickinson[30,31] provided a simple model to predict the network formation in a binary mixture of large and small spheres interacting either by a bridging mechanism or a depletion mechanism (depending on whether the strength of attraction between small and large particles is finite or negligible). His model[31] exhibited extreme sensitivity of the rheology of concentrated particulate dispersions and emulsions to the attraction interaction parameters. Although some previous theoretical models[32,33] and direct measurements[34–36] have demonstrated that for attractive force induced by an adsorbed polymer between inter-surface gaps, the range is of the order of radius of gyration of the added polymer and the strength is sensitive to the surface coverage. Bridging attraction is rarely taken as a short-range attraction model in the investigation of dynamical arrested behaviors of colloids. The main reason is that the bridging attraction is harder to quantitatively control.

A series of studies[28,29,37–39] have been carried out by our group using a mixed suspension of large hard spheres and small soft microgels with very well-defined bridging interaction to represent a simple particle to particle interaction potential, and thus to construct a new short-range attractive system. The system is composed of large hard polystyrene (PS) spheres and small soft poly(*N*-isopropylacrylamide) (PNIPAM) microgels in water. The PS spheres are stabilized in the solvent by a thin shell of covalently bonded poly(vinylpyrrolidone), which is a non-charged and water-soluble polymer. PNIPAM microgels are absorbable to the surface of PS spheres driven by the hydrophobic interaction.[40,41] At a given volume fraction of large PS spheres, gradually adding small microgel enhances the effective attraction strength between large particles until the attraction strength reaches a maximum value, after which adding more small particles slowly decrease the effective attraction strength. Since the size of the PNIPAM microgels is very small in comparison to the size of PS spheres, the pair-interaction potential between large spheres can be modelled using Baxter's[11] potential and extracted by using the neutron scattering technique.[28,29] By changing the mixing ratio and the total particle volume fraction, we obtained the state diagrams for the liquid–solid transition in this system.[29,37–39]

 This journal is © The Royal Society of Chemistry 2016

Published on 24 August 2016. Downloaded by National Institutes of Standards & Technology on 22/05/2017 20:20:39.

The small PNIPAM microgels are soft and deformable while sticking at the hard sphere surface. In this study, non-deformable hard cores are embedded into the PNIPAM microgels. We use microgels with a core–shell structure as bridging agents to trigger the aggregation and gelation behaviors, which will result in rigid bonds with different lengths. Microgels (instead of linear PNIPAM chains) are adopted because the bridging distance between the adjacent pair of large spheres can be tuned. The effects of the hard cores inside the microgels on the effective attraction between the large hard spheres are qualitatively discussed in this paper. We also quantitatively characterize the range and strength of attractive potentials during the shrinking of PNIPAM by using Baxter's one-component model. This study will help us to gain more detailed insights into the role of the attractive potentials on the liquid–solid transition in colloidal systems.

Experimental section

Materials

Styrene (98%, Sinopharm Chemical) was purified *via* passage through a basic alumina column to remove the inhibitor before use. Heavy water (D_2O, 99%, Alfa Aesar), *N*-isopropylacrylamide (NIPAM, 99%), 2,2′-azobisisobutyronitrile (AIBN, 98%, Tianjin Yuming), sodium dodecyl sulphate (SDS, 99%, Beijing Chemical), *N*,*N*′-methylenebisacrylamide (BIS, 99%, Alfa Aesar), ethanol (95%, Beijing Chemical), potassium peroxodisulfate (KPS, 99%, Sigma-Aldrich) and poly(vinylpyrrolidone) (PVP, M_w = 40 000 g mol^{-1}, Xilong Chemical) were all used without further purification. Water (H_2O) was obtained from a Milli-Q water purification system (Millipore, Bedford, MA, USA).

Synthesis and characterization

Four types of particles are used in this study, including large hard PS spheres and three types of small microgels. Monodispersed large PS spheres were synthesized through a one-stage suspension polymerization which has been described before.[37–39] The hydrodynamic radius (R_h) of PS microspheres determined by dynamic light scattering is about 1300 nm and the polydispersity index is about 1.06. Small microgel particles are named as S(0), S(50) and S(100), respectively. The number corresponds to the radius of the hard core inside the microgels. Therefore, S(0) is a pure soft microgel without a hard core. The S(0) microgel was synthesized following the procedure of Senff and Richtering[42] with recipes listed in Table 1. NIPAM (1.6 g), BIS (0.03 g) and SDS (0.03 g) were dissolved in 90 mL of water in a reaction flask. Argon was bubbled through the reaction mixture for 30 min. KPS (0.06 g) was dissolved in 10 mL of water and added into the flask. The reaction was continued at 70 °C for 8 h with agitation by a magnetic stirrer. The preparations of S(50) and S(100) microgels are briefly summarized as follows: first, the cores with radii of 50 nm and 100 nm were achieved *via* emulsion polymerization reported by Kim *et al.*[43] and Zhang *et al.*,[44] respectively; then, the shell layers were grown from the cores *via* seeded emulsion polymerization[43] with slight changes in the recipes (listed in Table 1). The resulting microgels were extensively dialyzed against water until its conductivity was less than 1 mS cm^{-1}. The core radius and the shell thickness were determined by dynamic light scattering (DLS), as shown in Fig. 1. The microgel particles are monodispersed with a polydispersity index less than 1.1. At the same temperature, the thickness of the PNIPAM layer (or the amount of the PNIPAM component) could be taken as an indicator of the softness of the microgel.

Table 1 Recipes for the preparation of small microgels and characterization

	Recipes							Characterization	
Name	NIPAM (g)	BIS (g)	Core (g)	KPS (g)	H_2O (mL)	T (°C)	t (h)	Core (nm)	Shell (nm)
S(0)	1.6	0.03	0	0.06	100	70	8	0	140
S(50)	1.85	0.126	1.38[a]	0.036	55	70	8	50	90
S(100)	0.5	0.035	1.38[b]	0.036	55	70	8	100	60

[a] Hard core with a radius of 50 nm. [b] Hard core with a radius of 100 nm.

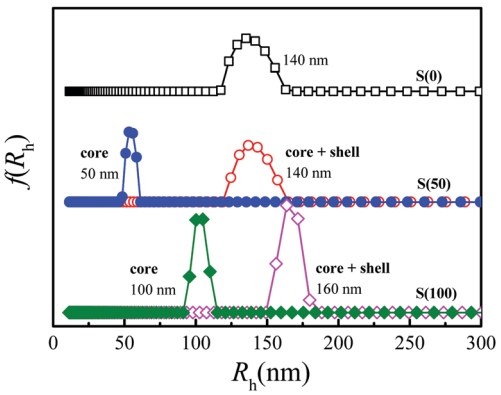

Fig. 1 Hydrodynamic radius distribution function, $f(R_h)$, of the cores and the microgels. Scattering angle θ = 30°; temperature T = 25 °C.

Preparation of mixed suspension

The solvent is a buoyancy-matching mixture of H_2O and D_2O with equal volumes to match the density of the PS large spheres and minimize the gravity-driven sedimentation. The bulk density of polystyrene (ρ = 1.05 g cm^{-3}) is used to calculate the volume fraction of large spheres Φ_L.

To determine the volume fraction of small microgels Φ_S, several dilute solutions of microgels were firstly prepared from the stock microgel suspensions with different dilution ratios (k). The relative viscosities (η_r) of these diluted suspensions were measured at 25 °C. An equation derived by Batchelor[45] was applied to relate the effective volume fraction (Φ_{eff}) of the dilute solutions with the measured η_r:

$$\eta_r = 1 + 2.5\Phi_{eff} + 5.9\Phi_{eff}^2 \quad (1)$$

Therefore, we obtained the relationship between Φ_{eff} and dilution ratio k. In our current study, $\Phi_S = \Phi_{eff}$ is assumed.

The powder of dry large spheres with mass W_L was dispersed in solvent in a 5.0 mL measuring flask. The suspension was

Published on 24 August 2016. Downloaded by National Institutes of Standards & Technology on 22/05/2017 20:20:39.

homogenized by ultrasonication at 25 °C for 30 minutes. A certain volume (V_S) of the small microgel solution was added to the suspension of large spheres, and solvent was added drop by drop until the fluid level reached the tick mark (V_{Tol} = 5.0 mL). Then, the mixed suspension was homogenized by ultrasonication at 25 °C for another 60 minutes. The Φ_L was calculated using $\Phi_L = (W_L/\rho)/V_{Tol}$, and Φ_S was known from the dilution ratio k with $k = V_S/V_{Tol}$.

It should be noted that eqn (1) is only applicable to dilute suspensions where multi-body interactions can be ignored and the swollen microgels can be modeled as hard spheres. The actual volume fraction of microgels is changed when mixing with large spheres due to adsorption and deformation, but Φ_S estimated from the hard sphere approximation is still used as a measure of the dosage of microgels in mixed suspensions in the present study, which will not affect the discussion.

Instrumentation

DLS was performed on a commercial laser light scattering spectrometer (ALV/DLS/SLS-5022F) equipped with a multi-τ digital time correlator (ALV5000) and a cylindrical 22 mW UNIPHASE He–Ne laser (λ = 632.8 nm). The baseline-normalized intensity–intensity time correlation function $g^{(2)}(t)$ in the self-beating mode was measured. The CONTIN program supplied with the correlator was used to calculate the hydrodynamic radius. The morphology of the dispersion at various states was probed by scanning electron microscopy (SEM). A JEOL (JSM 6700F) SEM operating at an accelerating voltage of 5 kV was used. A tiny drop of the dispersion was placed on a piece of silicon wafer and then water was removed by lyophilisation. In order to enhance conductivity, platinum was coated on each of the dried samples before SEM measurements. The rheological properties of the suspensions were investigated using a stress-controlled rheometer (Anton Paar MCR 502) with a 25 mm cone-plate geometry. The evaporation of solvent was minimized by coating silicon oil at the edge of the sample cell. As a standard protocol, a high strain dynamic shear rejuvenation (γ = 1000%, ω = 1 rad s^{-1}) was performed followed by a waiting time of typically 30 minutes before each experiment. Ultra-small angle neutron scattering (USANS) measurements were carried out at the U.S. National Institute of Standards and Technology (NIST) on a BT5 perfect crystal diffractometer. By using a neutron wavelength of 2.4 Å (6% $\Delta\lambda/\lambda$), a q-range of 0.00003–0.0026 $Å^{-1}$ was accessed (q is the scattering variable).[49] The samples were loaded into demountable titanium cells with a 1 mm path length. The data were reduced to the absolute scale and analyzed using the NIST-provided algorithms for WaveMetrics Igor Pro software.[50]

Results and discussions

1. Adsorption and bridging

It has been shown in our previous studies[37–39] that small soft microgels are readily adsorptive to the surface of large hard spheres when they are mixed together in water. At a constant volume fraction of large particles Φ_L, the volume fraction of small particles Φ_S is the key parameter in controlling the clustering and stabilizing behavior of the mixed suspension. A schematic illustration of clustering and stabilizing of the PS microspheres with the increasing volume fraction of small microgels has been proposed in our previous publication,[37] and we have redrawn it in the current paper as Fig. 2 for the reader's convenience. In the absence of small microgels, the large spheres are homogeneously dispersive in water. When a small amount of microgels is added to the suspension of large spheres, bridging clusters form, and the clusters first grow dramatically with the increasing Φ_S and then gradually dissolve when the Φ_S reaches a certain value Φ_S^*. With further increase of Φ_S to an over-saturated state, clusters re-appear. The reason has been taken as depletion attraction which we will not discuss much in this paper.

The clustering and re-stabilization behaviours of large hard spheres induced by three different small microgels are probed by DLS measurements as shown in Fig. 3. The legend on the right of each plot corresponds to the mixing ratio Φ_S/Φ_L. The appearance, gradual shifting to the larger and then smaller relaxation time (τ) direction, and eventual disappearance of a slow mode with the addition of microgels are observed in all three cases using different microgels. The fast mode has a characteristic time comparable to the diffusion of the isolated large particles, corresponding to the self-diffusion of the large hard spheres (or spheres with an adsorbed layer). The slow mode comes from the collective movement of colloidal particles bridged by microgels. The appearance and disappearance of the slow mode indicate the formation and dissolution of large aggregates, respectively, with the increasing concentration of microgels, which is consistent with stages 1–3 shown in the schematic of Fig. 2. Stage 4 (depletion cluster) is missing in the DLS data because to push the large particles with a very low concentration entering the depleting aggregation regime, a very

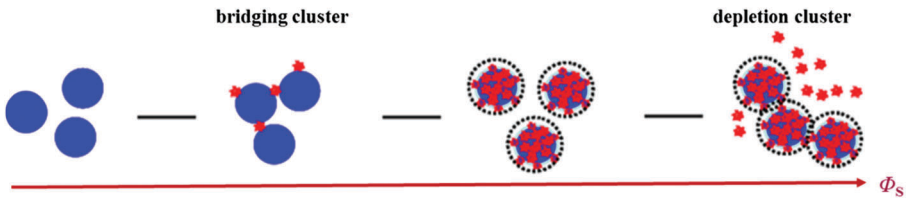

Fig. 2 A schematic illustration of clustering (or gelation) of large hard PS sphere with the increasing concentration of small soft microgels (Φ_S). The hard spheres, soft microgels and depletion layers are presented by blue, red and dotted circles, respectively.

 This journal is © The Royal Society of Chemistry 2016

Published on 24 August 2016. Downloaded by National Institutes of Standards & Technology on 22/05/2017 20:20:39.

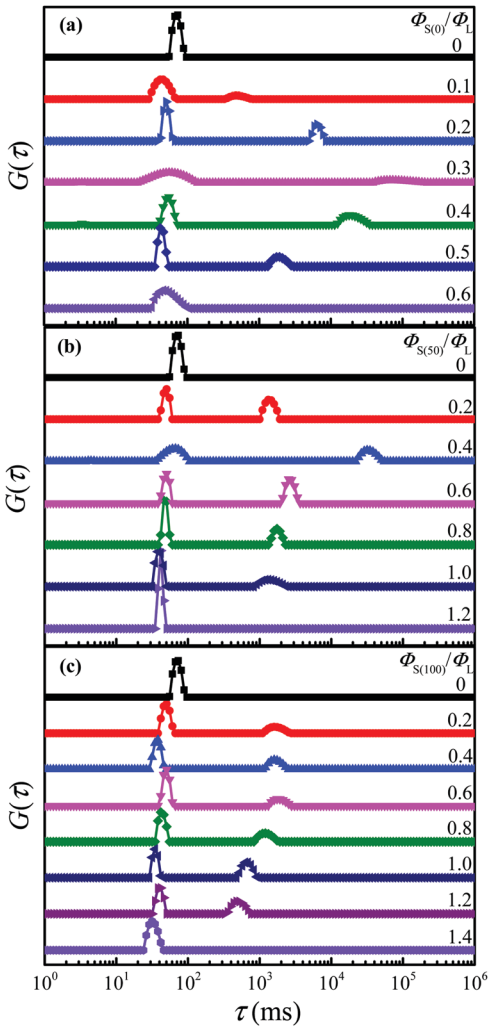

Fig. 3 Characteristic relaxation time distribution function $G(\tau)$ of suspensions with $\Phi_L = 1 \times 10^{-7}$ and various small microgels: (a) S(0); (b) S(50); (c) S(100). The distribution functions are shifted vertically along the Y-axis for clarity. The legend on the right of each plot corresponds to the mixing ratio Φ_S/Φ_L. All the measurements were carried out after the mixed samples have been equilibrated at 25 °C for 24 hours. The scattering angle is 30°.

high concentration of small particles is required. In that case, DLS measurements are not feasible anymore due to the multiple scattering at a high total concentration of particles. It should be noted that light scattering is more sensitive to large particles and aggregates, and the signal from small microgels may be screened due to their small size and low scattering contrast. Also, it should be pointed out that the characteristic relaxation time τ cannot be directly converted to the hydrodynamic radius of the diffusive objects *via* the Stokes–Einstein equation ($R_h = k_BT/6\pi\eta_0 D$) in the mixture cases, because the properties of the solvents (mixed with small particles) are unknown and the diffusion relationship $D = q^2\tau$ may not be satisfied for large clusters. (Here, k_B, T, and η_0 are the Boltzmann constant, the absolute temperature, and the solvent viscosity, respectively.) Therefore, the shifting of the fast mode to the small τ direction with the increasing concentration of small particles does not mean that the large particles become smaller, but the characteristic diffusion time becomes smaller in a more crowded environment due to more frequent collision. The adsorption of small microgels on the surface of hard spheres is reversible.[38]

The noteworthy differences in Fig. 3(a)–(c) are the amount of small microgels required to re-stabilize the same amount of large hard spheres and the characteristic relaxation time of the slow modes. The slow modes disappear at $\Phi_S/\Phi_L = 0.6$ for S(0), $\Phi_S/\Phi_L = 1.2$ for S(50), and $\Phi_S/\Phi_L = 1.4$ for S(100). More microgels with a thinner shell are required to fully cover and re-stabilize large hard spheres due to their weaker deformation ability and larger intrinsic occupied volume. Furthermore, when the characteristic relaxation time of the slowest mode induced by the three different small particles are compared (*i.e.* among $\Phi_S/\Phi_L = 0.3$ for S(0), $\Phi_S/\Phi_L = 0.4$ for S(50) and $\Phi_S/\Phi_L = 0.6$ for S(100)), it is clear that the order of magnitude significantly decreases as microgels with a thinner PNIPAM shell are used. These results imply a positive correlation between flocculation ability and particle softness. The softest particle, S(0), has the strongest flocculation ability.

The adsorption and bridging effect can also be visualized by SEM images. Pictures were taken under zero adsorption (Fig. 4 left), around half cover (Fig. 4 middle) and full cover conditions (Fig. 4 right). The surfaces of the pure large hard spheres are very smooth. The adsorbed S(0) and S(50) microgels evenly distribute on the surfaces of large hard spheres, and eventually their surfaces become fully covered by adsorbed microgel species at the monolayer level. Unlike the above mentioned soft microgels which are adsorbed tightly on the large microspheres, parts of the S(100) microgels have been are stripped off from the PS surface during the lyophilisation process in sample preparation. This in turn helps to explain that the S(100) microgels with the thinnest PNIPAM layer have the weakest affinity to the surface of large spheres. The bridging configuration can be easily identified in the softest microgel cases. The adsorbed softest S(0) microgels show a "fried egg-like structure", which is similar to what Destribats *et al.*[46] found in their study of the adsorption behavior of soft PNIPAM microgels at the oil-in-water emulsion interface. However, between the gaps of large particles, the S(0) microgels are torn and bridge the large particles making a standing network possible.

2. Gelation affected by core–shell particles

When Φ_L is large, the size of the aggregates induced by the addition of small particles can be so large to form percolated clusters. Therefore, the liquid-to-gel-to-liquid transitions will be observed. The characteristics of the sol and gel states are quantitatively analyzed by oscillatory frequency sweep measurements. Fig. 5 shows a set of typical data of storage moduli G' (filled symbols) and loss moduli G'' (open symbols) in mixtures with $\Phi_L = 0.30$ and various $\Phi_{S(50)}$. For samples without microgels ($\Phi_{S(50)}/\Phi_L = 0$, Fig. 5a), the G' and G'' can be scaled as $G' \sim \omega^2$ and $G'' \sim \omega$, which are typical characteristics of a viscoelastic liquid in the low frequency region. For mixtures with $0.004 \leq \Phi_{S(50)}/\Phi_L \leq 0.85$, rheological data reveals solid-like characters. G' is almost frequency-independent and $G' > G''$ in the experimental linear viscoelastic regime (0.1 rad $s^{-1} < \omega <$ 100 rad s^{-1}). It is clear that addition of

Published on 24 August 2016. Downloaded by National Institutes of Standards & Technology on 22/05/2017 20:20:39.

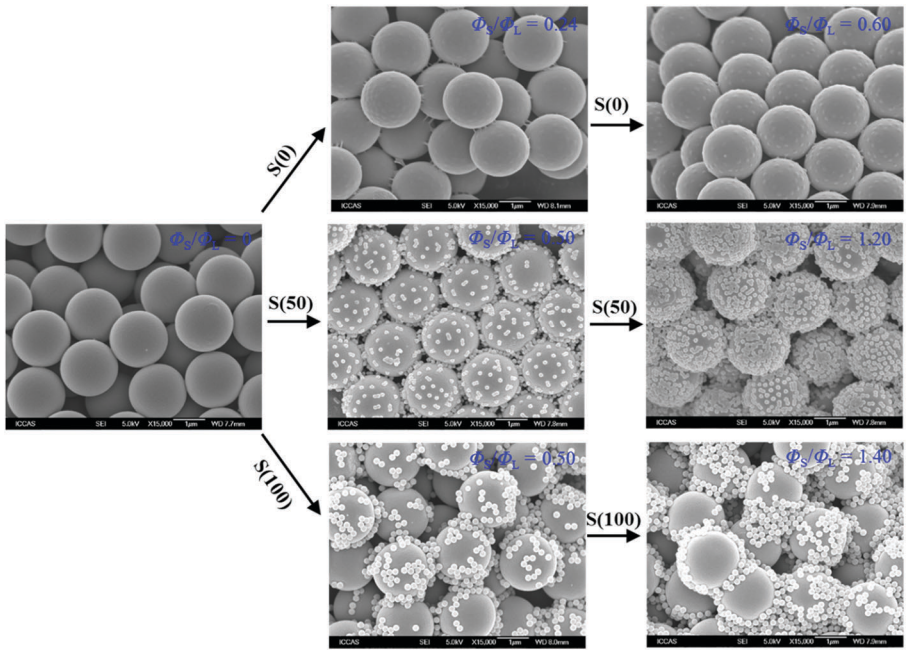

Fig. 4 SEM images of lyophilized suspensions with $\Phi_L = 2 \times 10^{-3}$ under various mixing conditions. The legends on the right top of each picture correspond to the mixing ratios Φ_S/Φ_L. All the samples have been stored at 25 °C overnight for equilibration before the lyophilisation process.

small particles first triggers a liquid-to-gel transition, and the gel becomes stronger with the increasing amount of small particles (Fig. 5a). Black symbols correspond to the liquid state (or the weakest gel state), and red symbols correspond to the gel state. The arrows indicate the direction of increasing $\Phi_{S(50)}$. Up to a certain value, increasing $\Phi_{S(50)}$ gradually weakens the gel (Fig. 5b). The gel becomes very weak at $\Phi_{S(50)}/\Phi_L = 0.95$. But further increasing the volume fraction of small particles, the mechanical response of the mixture becomes gradually stronger again (Fig. 5c). This is because it may intervene with the jamming effect at such a high total particle volume fraction, $\Phi_L + \Phi_S \geq 0.58$, and the system will go into the glass state. The transition from attractive gel (or attractive glass) to repulsive glass with the increasing volume fraction of small particles has been discussed in our previous paper.[39] The other reason could be, for this high value of Φ_L ($\Phi_L = 0.30$), at such a high value of $\Phi s_{(50)}$, there is just not enough 'free space' available to allow sufficient small particles to be added to large spheres to produce steric stabilization, and so gelation (*i.e.* percolation) remains instead. The effective steric stabilization only occurs when there is enough free volume in the system between all adjacent pairs of large particles to accommodate two complete layers of small particles in addition to the 'sink' of excess unadsorbed small particles.[31]

Typical oscillatory frequency sweep data for mixed suspensions of S(0) and S(100) are shown in the ESI† as Fig. S1 and S2, respectively. A liquid-to-gel-to-liquid transition is observed with increasing $\Phi_{S(0)}$, because S(0) is the softest and it will take less S(0) to fully cover the large particles. But a very weak gel state (or glass state?) remains at a high volume fraction of S(100), similar to the case of S(50) because the volume taken by the hard core of the microgel cannot be ignored anymore.

Once a percolated network structure is formed, the number density of bonds (bridges, connections) and the attractive interaction strength of each bond in the network are two key factors in determining the global rheological properties of the system. In our systems, PNIPAM is considered as a typical water-soluble polymer which bears both hydrophilic (amide) and hydrophobic (isopropyl and the backbone) groups. Hydrophobic interaction is considered to be the driving force for adsorption of microgels to the surface of large PS microspheres. As we can see in Fig. 4, a sphere-like soft microgel deforms into a "fried egg-like" structure after it was adsorbed to a hard surface. The deformation depends on the delicate balance between the intrinsic hydrophobicity of the NIPAM segments (which tends to favor the spreading of the microgels at the interface in order to increase the number of "hydrophobic" anchoring points) and the elastic resistance of the microgel particles (which is controlled by their internal structures, such as crosslinks and hard core). If we take the contribution from a single microgel as a bridge, then each microgel bridge may actually have multiple anchoring points on the microsphere surface which will the determine the strength and life time of each bridge. Therefore, at a constant Φ_L, as Φ_s is changed, not only the number of bridges will change, but also the strength of each bridge will change with the variation of the conformation of adsorbed microgels.

The storage modulus (at $\omega = 1$ rad s^{-1}) of gel samples induced by the three kinds of microgels, S(0), S(50) and S(100), are plotted in Fig. 6 as a function of the mixing ratio Φ_S/Φ_L. The volume fraction of large spheres is constant with $\Phi_L = 0.30$. Here, the criterion for the formation of the gel state is that, in small-amplitude oscillatory rheological measurements, the storage modulus G' ($G' > G''$) is almost constant and

 This journal is © The Royal Society of Chemistry 2016

Published on 24 August 2016. Downloaded by National Institutes of Standards & Technology on 22/05/2017 20:20:39.

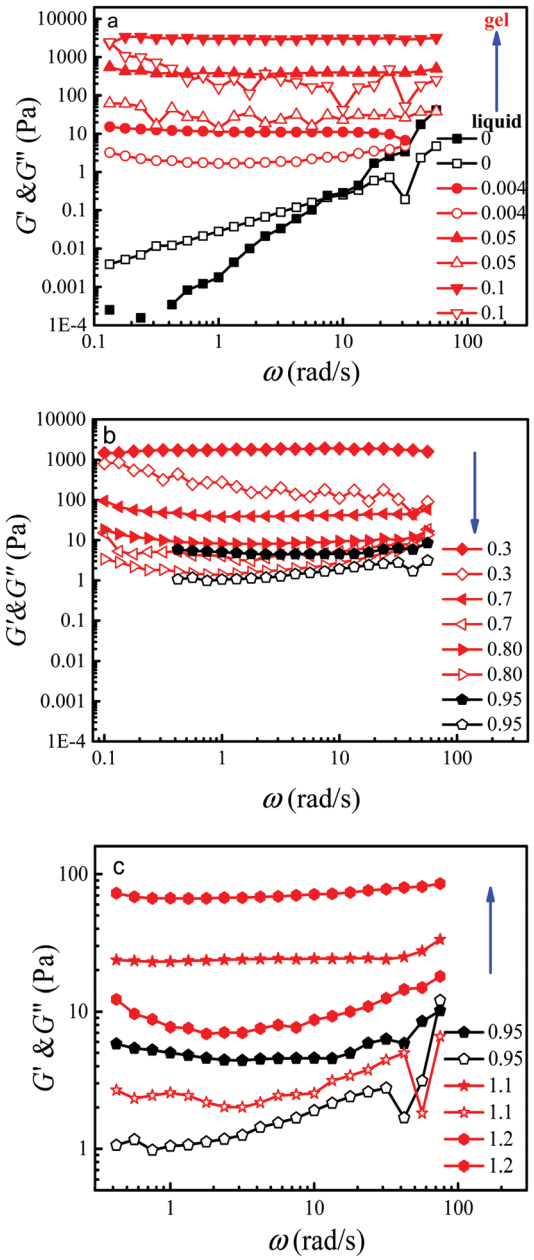

Fig. 5 Frequency sweep data for concentrated mixed suspensions with Φ_L = 0.30 at various volume fractions of S(50), $\Phi_{S(50)}$. The legends indicate the mixing ratio $\Phi_{S(50)}/\Phi_L$. Filled symbols correspond to the storage moduli G' and open symbols to loss moduli G''. The stress amplitude is set to σ = 0.1 Pa.

$G' > 10$ Pa in the experimental linear viscoelastic regime (0.1 rad $s^{-1} < \omega < 100$ rad s^{-1}). This method is widely adopted in determining the particle gel state.[47] The three plots show a similar feature that there is a G' maximum at a certain mixing ratio. The appearance of a maximum strength gel can be explained under the framework proposed by La Mer.[48] When two large spheres collide with each other, to form a bridge, the requirement is that the surface site of one sphere is covered by the microgel and the surface site of the other sphere remains uncovered. Therefore, the number density of bridges is proportional to $\theta(1 - \theta)$ with a maximum at θ = 0.5. Here, θ is the fraction of the surface covered by flocculants.

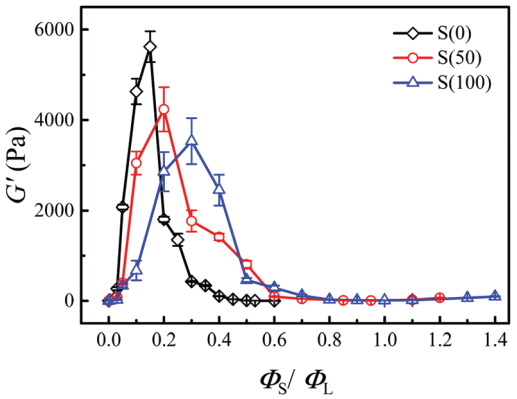

Fig. 6 The storage plateau modulus G' (at ω = 1 rad s^{-1}) of gel samples induced by S(0), S(50) and S(100). The volume fraction of large spheres is a constant with Φ_L = 0.30. Error bars correspond to one standard derivation estimated from three independent measurements.

If the conformation (thus the effective stickiness) caused by each microgel is constant under different mixing ratios of Φ_L and Φ_S, then symmetric parabolas would be expected in Fig. 6. However, the increase and the decay of the modulus around the maximum are asymmetric in Fig. 6. This asymmetry is related to the deformability of the microgels patching on the surface of large spheres. For the same type of microgel, the surface area (on large spheres) occupied by each adsorbed microgel will change with the dosage of the microgel added. Each microgel will tend to expand as much as possible and form a strong bridge at a low Φ_S where there is enough surface area for it to spread. But each adsorbed microgel may occupy less surface area at high Φ_S due to the competition of many microgels. Meanwhile, the system will approach a more crowded state where there is less free volume to allow the small particles to freely adjust their configuration.

The microgel with a larger core suffers more constraints from the hard core while deforming. Correspondingly, the rigid bridge formed by the core–shell microgel is weaker compared to that formed by the very soft microgel S(0). Therefore, the maximum G' achieved by using core–shell microgels decreases with the core size.

Based on the rheological criterion mentioned above, the gelation transition boundaries induced by the three types of microgels are identified on suspensions with Φ_L ranging from 0.01 to 0.35. The experimental state diagram of liquid-to-gel-to-liquid transitions in the (Φ_L, Φ_S) plane is shown in Fig. 7. For each type of microgel, at a given large particle concentration, there are two gelation transition concentrations for small particles. Therefore, there are low-Φ_S and high-Φ_S gelation lines, and they meet at a certain critical point (Φ_L*) below which no gelation transitions are observed. The reentrant weak gel (or glass) state induced by very high volume fractions of S(50) and S(100) is not considered here. In Fig. 7, inside the acute angle is the gel state, outside is the liquid state. The intrinsic excluded volume of S(0), S(50) and S(100) increases, and correspondingly, the deformability of S(0), S(50) and S(100) decreases. Therefore, just as expected, the gel boundaries shift

Published on 24 August 2016. Downloaded by National Institutes of Standards & Technology on 22/05/2017 20:20:39.

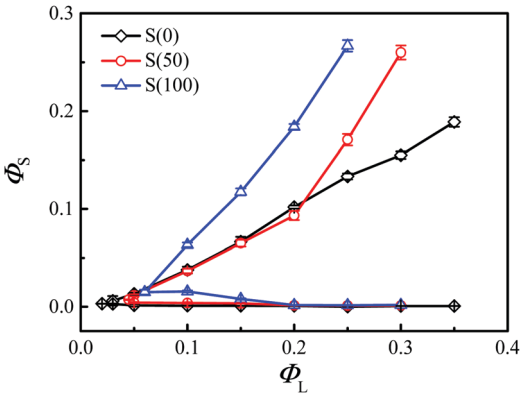

Fig. 7 Sol–gel state diagram of mixed suspensions of large PS particles and three types of small microgels determined by rheological measurements. The solid lines denote the upper and lower boundaries of the gel state. The sample with $G'(\omega) > G''(\omega)$, and $G'(\omega) > 10$ Pa is regarded as a gel, otherwise it is a liquid. Error bars correspond to one standard deviation estimated from three independent measurements.

to higher Φ_S directions as the PNIPAM shell becomes thinner, and the critical gelation concentration Φ_L^*, which is defined as the lowest Φ_L needed to form a percolation network, shifts to higher values as S(0), S(50) and S(100) are used. As we discussed before, each microgel bridge may have multiple anchoring points on the surface of large spheres, which is a factor determining the life time of a bridging bond. The other factor that affects the life time of a bridge is the concentration of large particles (the collision frequency between large spheres). For the breaking of a bridge all the anchoring points of a microgel should depart from one surface before two large spheres collide and reconnect again. To form a network, each large sphere is linked with several neighboring large spheres. Therefore, the life time of a network, which determines whether a system is a transient network or a permanent gel, depends not only on the lifetime of individual bridges but also on the particle volume fraction of the system. At a high degree of sphere–microgel stickiness, the addition of S(0) with a volume fraction of 0.3% is enough to produce a percolating network made of large spheres with a volume fraction of 3%. On the other hand, if the sphere–microgel stickiness is less strong, the addition of S(100) with a volume fraction of 1.5% leads to the gelation of large spheres with a volume fraction of 6%. At a low particle volume fraction, the system containing this same amount of S(100) is certainly well away from the sol–gel phase boundary.

3. Gelation affected by temperature

It is well-known that PNIPAM microgels are thermosensitive in aqueous solution: they will shrink when the temperature is increased above the volume phase transition temperature ($\approx$32 °C) due to dehydration. On the one hand, shrinking will definitely change the softness of the microgels. On the other hand, shrinking of microgels will also result in the change in surface coverage. The bridging mechanism is strongly related to the coverage of PNIPAM microgels on the surface of PS spheres. To form a bridge, it is a requirement that one surface site of the microsphere is covered by the microgel and another surface site remains uncovered. Therefore, we can tune the liquid–gel transition of mixed systems by changing the temperature. The temperature effect on gelation has been partly discussed in one of our previous papers,[38] where various transitions induced by changing the temperature have been demonstrated, including the transition from a weaker gel to a stronger gel, from a fluid to a bridging gel, and from a depletion gel to a bridging gel depending on the mixing ratio.

In this paper, we quantitatively characterize the strength and range of the effective attraction with increasing temperature. The USANS technique is applied and the data are analyzed by Baxter's one-component sticky hard-sphere model.[29] Only the mixtures with S(0) microgels are discussed here, because the analysis of data for S(50) and S(100) microgels will depend on the development of a two-component sticky hard-sphere model which is still ongoing. As we have shown before,[29] scattering from colloidal dispersions results from the difference in the scattering length density (SLD) between the particles and the surrounding medium, therefore the scattering contribution from the S(0) microgels can be neglected. The effects caused by the S(0) microgels can be indirectly incorporated into their influence on the effective interaction between the PS microspheres.

We consider a sample with $\Phi_L = 0.30$ and $\Phi_{S(0)} = 0.17$. At 20 °C, the surface of large spheres is fully covered by microgels and the system is in a dispersive liquid state (see the rheological data in Fig. S1, ESI†). The mixture experiences a liquid-to-gel transition as measured by small-amplitude oscillation during heating at a rate of 0.5 °C min^{-1} (inset of Fig. 8a). With increasing temperature, G' increases faster than G'' leading to a liquid-to-gel transition at $\approx$32 °C with $G' > G''$. The corresponding USANS data in the low q region ($q < 6.0 \times 10^{-4}$ Å^{-1}) at 20, 30 and 40 °C are shown in Fig. 8a. Symbols are experimental data points and solid lines are fitting curves based on Baxter's one-component sticky hard-sphere model after taking into account the instrument resolution. The fitting includes 7 parameters: volume fraction (Φ_L), radius of sphere (R_g = 9600 Å), SLD of sphere (1.4×10^{-6} Å^{-2}), SLD of solvent ($\sim 2.8 \times 10^{-6}$ Å^{-2}), perturbation parameter (ε), stickiness parameter (τ) and background. The background can be obtained from the asymptotic value at a large q as the scattering intensity is expected to follow the Porod law. Therefore, only ε (which characterizes the range of attraction) and τ (which characterizes the strength of attraction) are unconstrained variables in the fitting. The corresponding analyzed ε and τ values are plotted in Fig. 8b. For reference, the navy horizontal line with $\tau = 0.358$ is provided which corresponds to the percolation value at a volume fraction of 0.30 predicted by Baxter's model.[20] The strengthening of moduli with increasing temperature (Fig. 8a) is consistent with the gradual enhancement of effective interaction (as the stickiness parameter τ decreases in Fig. 8b). When gelation occurs, it follows a percolation mechanism, as the stickiness parameter τ goes down into the percolation region. Meanwhile, the perturbation parameter ε simultaneously decreases with increasing temperature, which indicates that the bridges are more compact due to shrinking.

 This journal is © The Royal Society of Chemistry 2016

Published on 24 August 2016. Downloaded by National Institutes of Standards & Technology on 22/05/2017 20:20:39.

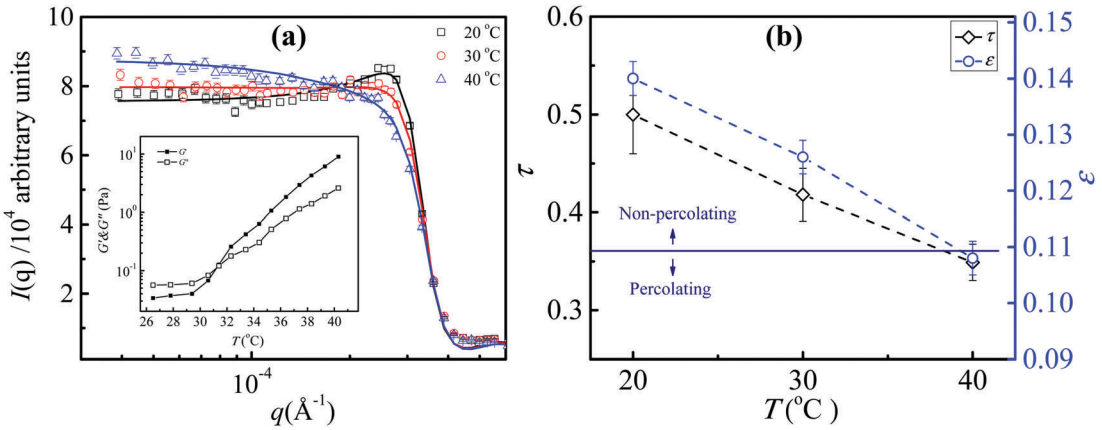

Fig. 8 (a) Experimental (symbols) and fit (solid lines) intensity data scattered from a suspension with Φ_L = 0.30 and Φ_S = 0.17 at 20 °C, 30 °C and 40 °C. Inset: Small-amplitude oscillatory measurements during heating (heating rate 0.5 °C min^{-1}) with a constant frequency ω = 1 rad s^{-1} and stress amplitude σ = 0.1 Pa. (b) The corresponding analyzed stickiness parameter τ and perturbation parameter ε *vs.* temperature T. Statistical error bars correspond to one standard deviation.

Conclusions

In summary, aggregation and gelation in mixed suspensions of large PS spheres and three types of small microgels were investigated in this study. At a rather low colloidal particle concentration, addition of small microgels leads to bridging flocculation, and then the system tends to re-stabilize at a high microgel concentration (*i.e.* sterically stabilized) because the particle surfaces become fully saturated at the monolayer level by the adsorbing microgel species. At a high colloidal particle concentration, the bridging effect leads to a liquid–solid transition. The sol–gel transitions induced by the addition of the three types of small microgels are carefully mapped out *via* a rheological method and compared. It was found that softer microgels are adsorbed more tightly by deforming laterally across the surface of large PS spheres, and hence create stronger bridges between two large spheres which are conducive to support a space-spanning network. Since the sizes of the microgels are very small in comparison to the size of the PS hard spheres, the bridging effects caused by the microgels can be incorporated into their influence on the effective attraction interaction between the large hard spheres and represented by a short-range attraction potential. Our efforts are devoted to tune the attractive interaction between the small microgels and large spheres and investigate its effect on the gelation behaviours. Our goal is to fill the gap between the strong bridging attraction system and the depletion attraction system. This work opens a way to control interparticle interactions and may be exploited to design materials of controllable strength. More investigations are needed in the future, such as quantitative characterization of the effective attraction between large spheres and core–shell microgels by scattering and other techniques.

Acknowledgements

This work is supported by the Chinese National Science Foundation (Project 21474121) and the National Basic Research Program of China (973 Program, 2012CB821503). Certain commercial equipment, instruments, or materials (or suppliers or software *etc.*) are identified in this paper to foster understanding. Such identification does not imply recommendation or endorsement by the U.S. National Institute of Standards and Technology, nor does it imply that the materials or equipment identified are necessarily the best available for the purpose.

References

1 K. A. Dawson, *Curr. Opin. Colloid Interface Sci.*, 2002, **7**, 218–227.
2 V. Trappe and P. Sandkühler, *Curr. Opin. Colloid Interface Sci.*, 2004, **8**, 494–500.
3 M. H. J. Hagen and D. Frenkel, *J. Chem. Phys.*, 1994, **101**, 4093–4097.
4 E. J. Meijer and F. E. Azhar, *J. Chem. Phys.*, 1997, **106**, 4678–4683.
5 E. Lomba and N. G. Almarza, *J. Chem. Phys.*, 1994, **100**, 8367–8372.
6 M. Dijkstra, *Phys. Rev. E: Stat., Nonlinear, Soft Matter Phys.*, 2002, **66**, 021402.
7 S. Asakura and F. Oosawa, *J. Polym. Sci.*, 1958, **33**, 183–192.
8 A. Vrij, *Pure Appl. Chem.*, 1976, **48**, 471–483.
9 P. R. ten Wolde and F. Daan, *Science*, 1997, **277**, 1975–1978.
10 G. A. Vliegenthart, J. F. M. Lodge and H. N. W. Lekkerkerker, *Phys. A*, 1999, **263**, 378–388.
11 R. J. Baxter, *J. Chem. Phys.*, 1968, **49**, 2770–2774.
12 Y. C. Chiew and E. D. Glandt, *J. Phys. A: Math. Gen.*, 1983, **16**, 2599–2608.
13 M. A. Miller and D. Frenkel, *J. Chem. Phys.*, 2004, **121**, 535–545.
14 J. A. Barker and D. Henderson, *Rev. Mod. Phys.*, 1976, **48**, 587–671.
15 M. G. Noro and D. Frenkel, *J. Chem. Phys.*, 2000, **113**, 2941–2944.

Published on 24 August 2016. Downloaded by National Institutes of Standards & Technology on 22/05/2017 20:20:39.

16 A. Malijevsky, S. B. Yuste and A. Santos, *J. Chem. Phys.*, 2006, **125**, 074507.
17 N. E. Valadez-Perez, A. L. Benavides, E. Scholl-Paschinger and R. Castaneda-Priego, *J. Chem. Phys.*, 2012, **137**, 084905.
18 G. Foffi, C. De Michele, F. Sciortino and P. Tartaglia, *Phys. Rev. Lett.*, 2005, **94**, 078301.
19 A. H. Krall and D. A. Weitz, *Phys. Rev. Lett.*, 1998, **80**, 778–781.
20 H. Verduin and J. K. G. Dhont, *J. Colloid Interface Sci.*, 1995, **172**, 425–437.
21 A. Woutersen, R. P. May and C. G. Dekruif, *J. Colloid Interface Sci.*, 1992, **151**, 410–420.
22 A. P. Eberle, R. Castaneda-Priego, J. M. Kim and N. J. Wagner, *Langmuir*, 2012, **28**, 1866–1878.
23 M. L. Broide, T. M. Tominc and M. D. Saxowsky, *Phys. Rev. E: Stat. Phys., Plasmas, Fluids, Relat. Interdiscip. Top.*, 1996, **53**, 6325–6335.
24 F. Cardinaux, T. Gibaud, A. Stradner and P. Schurtenberger, *Phys. Rev. Lett.*, 2007, **99**, 118301.
25 W. C. K. Poon, A. D. Pirie, M. D. Haw and P. N. Pusey, *Phys. A*, 1997, **235**, 110–119.
26 P. J. Lu, E. Zaccarelli, F. Ciulla, A. B. Schofield, F. Sciortino and D. A. Weitz, *Nature*, 2008, **453**, 499–503.
27 E. Zaccarelli, *J. Phys.: Condens. Matter*, 2007, **19**, 323101.
28 G. Yuan, J. Luo, C. C. Han and Y. Liu, *Phys. Rev. Lett.*, submitted.
29 J. Luo, G. Yuan, C. Zhao, C. C. Han, J. Chen and Y. Liu, *Soft Matter*, 2015, **11**, 2494–2503.
30 E. Dickinson, *J. Colloid Interface Sci.*, 1989, **132**, 274–278.
31 E. Dickinson, *J. Chem. Soc., Faraday Trans.*, 1995, **91**, 4413–4417.
32 J. Klein and P. Pincus, *Macromolecules*, 1982, **15**, 1129–1135.
33 G. J. Fleer, J. M. H. M. Scheutjens and M. A. C. Stuart, *Colloids Surf.*, 1988, **31**, 1–29.
34 J. N. Israelachvili, M. Tirrell, J. Klein and Y. Almog, *Macromolecules*, 1984, **17**, 204–209.
35 J. Klein and P. F. Luckham, *Nature*, 1984, **308**, 836–837.
36 S. S. Patel and M. Tirrell, *Annu. Rev. Phys. Chem.*, 1989, **40**, 597–635.
37 C. Zhao, G. Yuan, D. Jia and C. C. Han, *Soft Matter*, 2012, **8**, 7036–7043.
38 C. Zhao, G. Yuan and C. C. Han, *Macromolecules*, 2012, **45**, 9468–9474.
39 C. Zhao, G. Yuan and C. C. Han, *Soft Matter*, 2014, **10**, 8905–8912.
40 J. Gao and C. Wu, *Macromolecules*, 1997, **30**, 6873–6876.
41 T. Hu, J. Gao, C. Wu, H. Auweter and R. Iden, *J. Phys. Chem. B*, 2002, **106**, 9815–9819.
42 H. Senff and W. Richtering, *J. Chem. Phys.*, 1999, **111**, 1705–1711.
43 J. H. Kim and M. Ballauff, *Colloid Polym. Sci.*, 1999, **277**, 1210–1214.
44 F. Zhang and C.-C. Wang, *Colloid Polym. Sci.*, 2008, **286**, 889–895.
45 G. K. Batchelor, *J. Fluid Mech.*, 1977, **83**, 97–117.
46 M. Destribats, V. Lapeyre, M. Wolfs, E. Sellier, F. Leal-Calderon, V. Ravaine and V. Schmitt, *Soft Matter*, 2011, **7**, 7689–7698.
47 M. Laurati, G. Petekidis, N. Koumakis, F. Cardinaux, A. B. Schofield, J. M. Brader, M. Fuchs and S. U. Egelhaaf, *J. Chem. Phys.*, 2009, **130**, 134907.
48 V. K. La Mer, *Discuss. Faraday Soc.*, 1966, **42**, 248–254.
49 J. G. Barker, C. J. Glinka, J. J. Moyer, M. H. Kim, A. R. Drews and M. Agamalian, *J. Appl. Crystallogr.*, 2005, **38**, 1004–1011.
50 S. R. Kline, *J. Appl. Crystallogr.*, 2006, **39**, 895–900.

 This journal is © The Royal Society of Chemistry 2016